Understanding the Solution Chemistry of Lead Halide Perovskites Precursors

Eros Radicchi,[a,b] Edoardo Mosconi,[b] Fausto Elisei,[a,c,*] Francesca Nunzi,[a,b,*] Filippo De Angelis [a,b,d]

[a] Department of Chemistry, Biology and Biotechnology, University of Perugia, via Elce di Sotto 8, I-06123 Perugia, Italy.

[b] Computational Laboratory of Hybrid/Organic Photovoltaics (CLHYO), CNR-ISTM, via Elce di Sotto 8, I-06123 Perugia, Italy.

[c] Center of Excellence on Innovative Nanostructured Materials (CEMIN), University of Perugia, via Elce di Sotto, 8, I-06123 Perugia, Italy.

[d] CompuNet, Istituto Italiano di Tecnologia, Via Morego 30, 16163 Genova, Italy.

Corresponding Author *E-mail: fausto.elisei@unipg.it; francesca.nunzi@unipg.it

Abstract

Identifying the composition of the solvated iodoplumbate complexes that are involved in the synthesis of perovskites in different solution environments is of great relevance in order to link the type and quantity of precursors to the final optoelectronic properties of the material. In this paper we clarify the nature of these species and the involved solution equilibria by combining experimental analysis and high-level theoretical calculations, focusing in particular on the DMSO and DMF solvents, largely employed in the perovskites synthesis. The specific molecular interactions between the iodoplumbate complexes, $[PbI_m]^{2-m}$, and the solvent molecules, X, were analyzed by identifying the most thermodynamically stable structures in various solvent solutions and characterizing their optical properties trough DFT and TD-DFT calculations. A comparison with the experimental UV-Vis absorption spectra allows for the first time the definition of the number of iodide and solvent ligands bonded to the Pb^{2+} ion and of the complex formation constants of the involved species.

1. Introduction

Lead halide perovskites (LHPs) show outstanding optoelectronic properties, that have allowed the production of highly efficient solar cells,[1–3] rivaling with established technologies. A significant point of strength for LHPs is that they can be efficiently synthesized by cheap solution-based methods,[4–8] starting from common materials, such as PbI_2 and methylammonium iodide (MAI) in an appropriate coordinating solvent, typically dimethylsulfoxide (DMSO), dimethylformamide (DMF), γ-butyrolactone (GBL), acetonitrile (ACN) or a combination thereof.

The basic LHPs synthesis is surprisingly simple: mixing a metal-halide precursor solution (*e.g.* a concentrated solution of PbI_2) with a 1:1 halide salt containing the A-cation (*e.g.* MAI) and evaporating the solvent gives a polycrystalline $MAPbI_3$ thin film, Eq. 1:

$$[(PbI_2)\text{-}solv_n]_{solv} + (MAI)_{solv} \rightarrow (MAPbI_3)_{solid} + solv_{gas} \qquad (1)$$
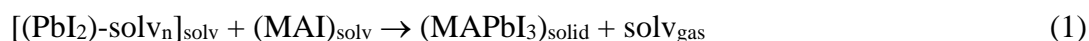
The apparent simplicity of the synthesis, however, should not be taken as the underlying physico-chemical processes being similarly simple, since they involve the solvation/desolvation and complexation equilibria of all the participating species. Many variables have to be taken into account when dealing with these solution-based synthesis methods. It has been proven that changing any synthesis parameter, such as the precursors concentration and stoichiometry, and the nature of the solvent may lead to perovskites with different structural, electronic and optical properties, that finally affect the ensuing solar cell efficiency and stability.[9–26] A plethora of different approaches have been implemented to improve the quality of the perovskite thin films, including change of the precursor stoichiometry,[9] use of different lead salts,[10] change of the halide [11,12,21–23] and use of solvent engineering tecnhiques.[13–15,24–26]

The nature of the solvent can affect the final material quality both in terms of crystallization rate and formation of solid state intermediates from the precursors, which have been characterized by means of X-ray powder diffraction and other structural analysis in DMSO,[24,27] DMF[28,29] and

3

GBL[30] solvents. Moreover, some synthetic routes for highly efficient perovskites employ antisolvents[31,32] (*e.g.* chlorobenzene or toluene) and the treatment of precursors solution with additives, such as hexamethylphosphoramide[33] and 1,3-dimethyl-2-imidazolidinone,[34] as well as the use of solvent blends.[35] Various studies have been carried out on the solution chemistry of the perovskite precursors,[16,36–45] highlighting the primary role of the coordinating solvent in the formation of iodoplumbate species in typical synthetic solution environment. Nevertheless, no clear evidence of the specific structures of the solvated iodoplumbate is provided, rather a sort of correlation between specific solvent properties (e.g. dielectric constant, polarity, Gutmann's donor ability, Mayer bond order, coordinative power) and feasible iodoplumbate complexes are generally supplied. At present the nature of the iodoplumbate species formed in the perovskite precursor solution, specifically the coordination number of the possible Pb^{2+} complexes, in terms of both iodide and solvent coordinated ligands, and the selective role of different coordinating solvents has not been fully understood.

Accordingly, in the present manuscript we investigate the chemistry of typical precursor solutions employed for LHPs synthesis by a combined experimental and computational approach. In particular, we study the properties of both $Pb(NO_3)_2$ and PbI_2 solutions in DMSO, without and with the addition of MAI, and we then extend the same analysis to a PbI_2 solution in DMF. By comparing the calculated energetics and UV-Vis spectra of several possible intermediates, $[PbI_mX_n]^{2-m}$ (X=DMSO, DMF), to the experimental absorption profiles of different solutions with and without added MAI, we identify, for each solvent, the species effectively involved in the perovskite precursor solution, characterizing the iodide and solvent coordination number and the structural and optical properties. A general trend based on the coordinative power of different solvents in forming different iodoplumbates is obtained. Our results show how the solvent profoundly affects the nature of the LHP precursor solution, in terms of lead coordination number

and stability of different solvent/halide lead complexes, possibly providing important information on how to further optimize the perovskite synthetic conditions.

2. Methods

2.1 Computational details

We investigate a series of $[PbI_mX_n]^{2-m}$ complexes (where m=0-4, n=0-7, and X=DMSO, DMF, GBL, ACN). The molecular and electronic structure calculations were performed within density functional theory (DFT) using the Gaussian 09[46] software package, using the LANL2DZ basis set for heavy Pb and also for I atoms together with the LANL2 pseudopotentials for the core electrons, while for light atoms (C, H, N, O, S) we employed the 6-31G* basis sets. The ADF 2014.04 program package[47–49] has been used for the time dependent (TD) DFT calculations together with a Slater type TZP basis set for all the atoms (the cores 1s-4p and 1s-4d were kept frozen, respectively for I and Pb) and a ZORA Hamiltonian to include relativistic spin-orbit coupling (SOC) effects.[50,51] In both cases we recurred to the B3LYP exchange-correlation functional.[52–55] Solvents considered in this work were simulated both with implicit solvation models (polarizable continuum model, PCM in Gaussian09 and COSMO in ADF 2014.04) and adding explicit coordinative molecules, that is necessary to investigate for the particular chemical interactions that we are interested in. The effect of the coordinative solvent on the various iodoplumbate complexes $[PbI_mX_n]^{2-m}$ has been deeply investigated evaluating the energetics of the complexes for different solvents, using the following equation:

$$E_{rel} = \frac{E_{tot} - E_{iodo} - E_{solv}*n}{n} \qquad (2)$$

where E_{tot} is the total energy of the $[PbI_mX_n]^{2-m}$ system, E_{iodo} and E_{solv} are, respectively, the energy of the unsolvated iodoplumbate $[PbI_m]^{2-m}$ and of the solvent molecule X, and n is the number of explicit coordinating solvent molecules of X.

The absorption spectra have been simulated by interpolating the computed electronic transitions by Gaussian functions with a broadening $\sigma=0.01$ eV.

2.2 Experimental details

Solutions of $Pb(NO_3)_2$ 0.1 mM in DMSO and PbI_2 0.24 mM in DMF were prepared, while in GBL and ACN solvents we could not attain the lead salt dissolution. MAI solutions in DMF and in DMSO were prepared and added to the reaction container with a 2-20 μL and a 20-200 μL Rainin Pipet-lite™ micropipette in order to obtain Pb:MAI mole ratio ranging from 1:2 to 1:152 / 1:1 to 1:150 in DMSO / DMF solvent. Moreover, PbI_2 solutions with concentrations ranging from 0.05 to 0.50 mM in DMSO were prepared. PbI_2 0.24 mM + MAI solutions in a 1:5 ratio were prepared both in GBL and ACN solvents in order to obtain the complete dissolution of the lead salt. Further MAI were added from a 0.1 M solution with a 20-200 μL Rainin Pipet-lite™ micropipette. UV-Vis absorption spectra were recorded with a double beam spectrophotometer *Perkin-Elmer Lambda 800* at each addition of MAI, employing quartz cuvettes with two optical walls and an optical path of 1.0 or 0.5 cm. In order to determine the equilibrium constants as well as the concentration profiles and the spectra of intermediate species, the global fitting of multivariate spectrophotometric data was carried out by employing the ReactLab™ EQUILIBRIA[56] software (Jplus Consulting). The parameters sum-of-squares and deviation standard for the residuals were used to evaluate the goodness of the fits. $Pb(NO_3)_2$ 1 mM in DMSO and 0.1 mM in DMF were also prepared and added with MAI with different Pb:MAI mole ratio in order to supply data for a more complete EQUILIBRIA analysis.

3. Results and Discussion

It is well established that Pb^{2+} ions readily undergo complexation with halides ions and that coordinative solvents are able to donate a pair of electrons to form Lewis adducts with the metal

centre.[36] The coordinative solvents are expected to play a key role on the stabilization of the various iodoplumbates in the precursor solution. We first registered the UV-Vis absorption spectra of the $Pb(NO_3)_2$ / PbI_2 salts in DMSO / DMF solvents, to then examine the effect on the absorption spectra of the addition of MAI in different concentrations. The PbI_2 salt is expected to dissociate in PbI^+ and Pb^{2+} ions, while upon incremental addition of I^- in solution, it also equilibrates with various iodoplumbate species (e.g. PbI_3^-, PbI_4^{2-}), giving rise to a complex solution chemistry. The measured UV-Vis spectra of PbI_2 in DMSO (see Figure S2 and Table S2 in SI) confirm the dissociation of PbI_2, according to the Lambert-Beer law. Therefore, in order to eliminate possible uncertainties on the starting solution composition, we decided to employ $Pb(NO_3)_2$ solutions as lead source. $Pb(NO_3)_2$ is completely dissociated into free ions in DMSO, based on the agreement of measured UV-Vis spectra with the Lambert-Beer law (see Table S1 in SI). The UV-Vis spectrum $Pb(NO_3)_2$ in DMSO (Figure 1a) shows one peak, centered at 257 nm, that can be assigned to the solvated Pb^{2+} ion. By adding increasing concentration of MAI to the solution, the solvated Pb^{2+} peak slightly shifts and its intensity increases, while two new bands at 290 and 320 nm raise, thus pointing at the appearance of different iodoplumbate species, in agreement with Stewart *et al.*[37]. Further absorption spectra for $Pb(NO_3)_2$ solutions with different salt concentrations (*i.e.* 0.1 and 1 mM) and with Pb:MAI concentrations ratio beyond 1:152 were also registered. The overall data were analyzed for the definition of the spectral shapes and complex formation constants of the involved species. The equilibrium constants for the hypothesized $[PbI_mX_n]^{2-m}$ complexes are reported in Table 1, showing that PbI^+ and PbI_2 species are thermodynamically favored with respect to PbI_3^- and PbI_4^{2-} both in DMSO and DMF solvents, even if with different magnitude: the formation of iodoplumbates with an high content of iodide is in fact favored in the less coordinative solvent. Since we could not elaborate the formation constant value of the PbI_4^{2-} complex, we included in Table 1 the results from Manser *et al.*,[36] that agree pretty well with the reported PbI_3^- formation constant value. The elaborated spectra, Figure S2 in SI, show that PbI^+ and PbI_2 have a

similar absorption maximum (287 vs 290 nm), though the latter has a higher molar absorption coefficient.
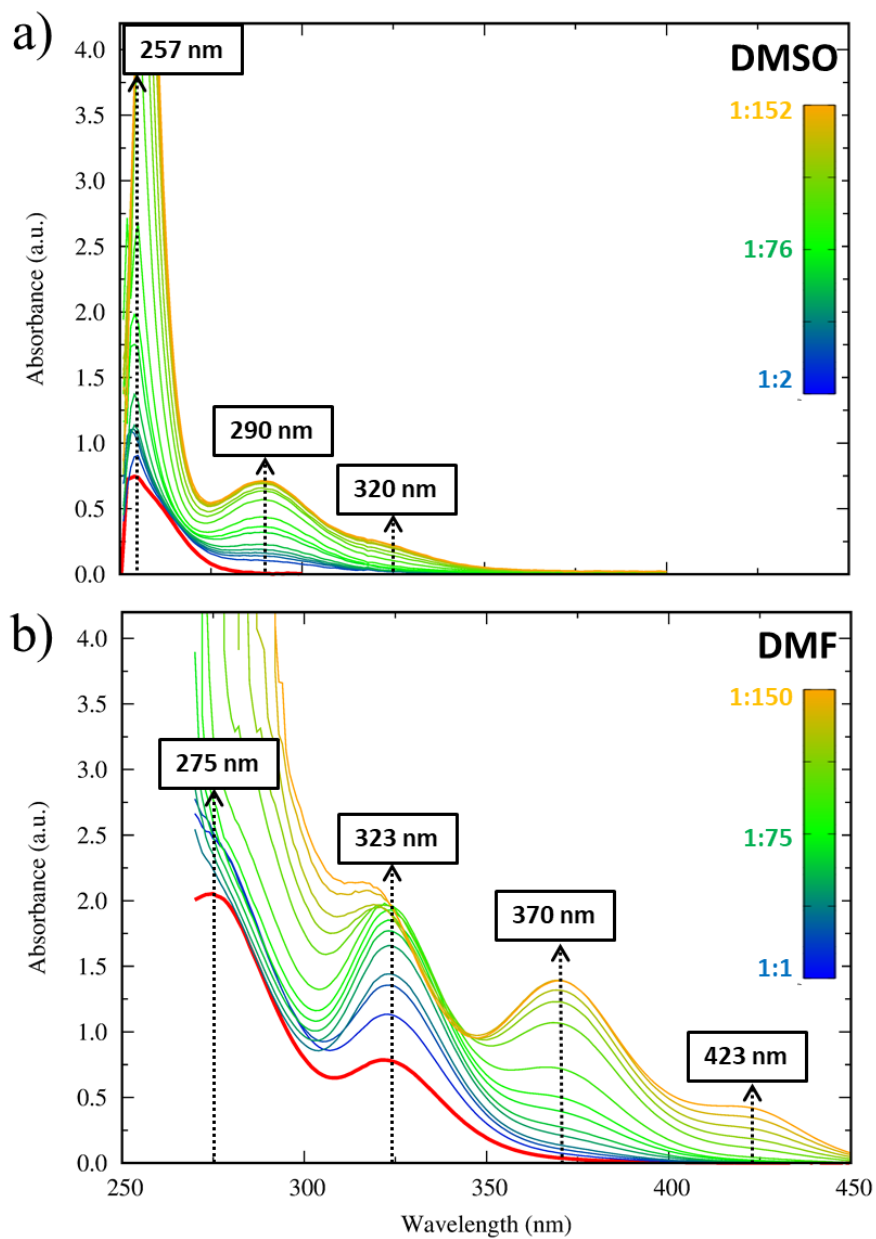
Figure 1. UV-Vis absorption spectra of a) solutions of Pb(NO$_3$)$_2$ 0.1 mM in DMSO and b) PbI$_2$ 0.24 mM in DMF – red solid lines – and with increasing concentration of MAI – colored lines. Pb:MAI mole ratio from 1:2 to 1:152 in DMSO and from 1:1 to 1:150 in DMF. The arrows point at the absorption maxima positions.

Table 1. Formation constants for the $[PbI_mX_n]^{2-m}$ complexes hypothesized in the $Pb(NO_3)_2$ + MAI solution in DMSO and in DMF solvents elaborated with ReactLab™ EQUILIBRIA.[49] [a] Data from Manser et al.[36].

	DMSO	DMF	DMF [a]
complex formation	log K	log K	log K
$Pb^{2+} + I^- \rightarrow PbI^+$	3.877 ± 0.095	3.443 ± 0.044	/
$PbI^+ + I^- \rightarrow PbI_2$	3.140 ± 0.017	2.228 ± 0.076	/
$PbI_2 + I^- \rightarrow PbI_3^-$	0.988 ± 0.045	2.050 ± 0.071	1.732
$PbI_3^- + I^- \rightarrow PbI_4^{2-}$	0.719 ± 0.052	/	0.778

The UV-Vis spectrum of a PbI_2 solution in DMF (Figure 1b) shows markedly different features. The pristine solution spectrum shows two peaks, at 275 and 323 nm, which are possibly related to solvated PbI^+ or PbI_2 species or a combination of the two. Upon MAI addition, besides an intensity raising of the aforementioned bands, two new peaks with lower intensity emerge up to the visible region, specifically at 370 and 423 nm, pointing at the formation of other iodoplumbate complexes, enriched with iodine, such as PbI_3^- or PbI_4^{2-}. This is in agreement with Manser et al.[36].

PbI_2 was not completely dissolved in GBL and ACN solvents; these solutions remained opalescent indicative of aggregation and other related phenomena, so that the UV-Vis spectra could not be registered in a reproducible way. This did not allow to carry out a comparable investigation of PbI_2 in GBL and ACN as was done for DMSO and DMF. To bypass this problem, we directly considered the UV-Vis spectra of PbI_2 + MAI solutions in a 1:5 ratio, that resulted completely dissolved due to the formation of the soluble PbI_3^- and PbI_4^{2-} iodoplumbates. The presence of these complexes is highlighted by the typical absorption features registered at 370 and 423 nm, in analogy with the DMF solvent. The further addition of 50, 100, 150 and 200 μL of MAI 0.1 M confirms this same trend (see Figures S3 and S4 in SI).[36] The further addition of 50, 100, 150 and 200 μL of MAI 0.1 M confirms this same trend (see Figures S3 and S4 in SI).

Comparing the spectral evolution in different solvents, we can conclude that the employed solvent strongly affects the solution chemistry of the solvated Pb^{2+} ion and its interaction with added MAI, giving rise to different solvated iodoplumbate complexes with different relative

composition, of the type $[PbI_mX_n]^{2-m}$, with X=solvent. On the basis of recent works,[36,37] we assign the peaks at 290/323 and 320/370 nm in DMSO/DMF to the PbI_2 and PbI_3^- species, respectively, as reported in Table 2. In DMF a third iodoplumbate complex, PbI_4^{2-}, is present, related to the peak at 423 nm, which apparently is not observed in DMSO. In the same way, the low coordinative GBL and ACN solvents show the PbI_3^- and PbI_4^{2-} absorption features respectively at 370/423 nm. In the same way, the low coordinative GBL and ACN solvents show PbI_3^- and PbI_4^{2-} absorption features respectively at 370/423 nm. Due to the fact that MAI was added to the reaction container before the spectra were registered, we cannot unambiguously assign the other absorption peaks to the Pb^{2+}, PbI^+ and PbI_2 case as done for DMSO/DMF. Comparing our data with previous experimental works,[40,57] we notice how the UV-vis spectra are shifted to lower wavelengths when more coordinative solvents are employed.

Table 2. Absorption maxima (nm) of experimental UV-Vis spectra of $Pb(NO_3)_2$ + MAI in DMSO and PbI_2 + MAI in DMF, GBL and ACN solutions.

	DMSO	DMF	GBL	ACN
Pb^{2+}	257	/	/	/
PbI^+	287	/	/	/
PbI_2	290	323	/	/
PbI_3^-	320	370	370	370
PbI_4^{2-}	/	423	423	423

The strong influence of the solvent on the optical properties of the Pb^{2+} complexes can be attributed to several factors, such as an intrinsic solvent effect (solvatochromism), a change in the number of coordinating solvent molecules for a given iodide complex, the different ability of the solvents to dissociate PbI_2[58] or a combination thereof. The complexity of the iodoplumbate systems and of the involved equilibria pushed us to resort to the use of DFT calculations for the determination of the most thermodynamically stable iodoplumbates in various solvent solutions and of their optical

properties: besides DMSO and DMF, we explored also the complexes with GBL and ACN for a wider understanding of the solvent effect.
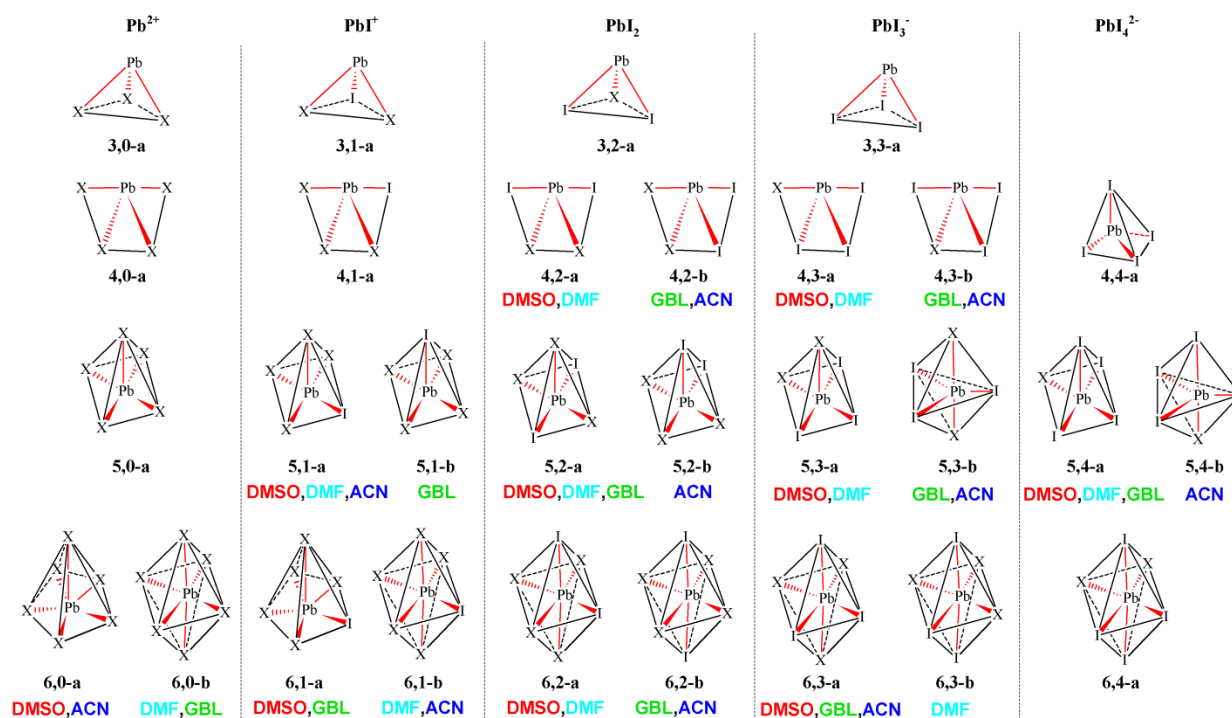
Scheme 1. $[PbI_mX_n]^{2-m}$ (X=solvent) most stable coordination, each row referring to a selected coordination number. Each structure is labelled as **cn,m-a/b**, where **cn** is the coordination number, **m** counts the iodine atoms and **a/b** refers to different configurations.

Because of the marked effect of the solvent on the iodoplumbates optical properties, we first consider the coordination complexes of the bare Pb^{2+} ion with the DMSO solvent molecules and we benchmarked the employed computational strategy by comparison with the experimental spectrum of the $Pb(NO_3)_2$ salt in DMSO. Specifically, we considered $[PbX_n]^{2+}$ complexes with n varying between 3 and 6. Two distinct structural categories of coordination geometries for the Pb^{2+} ion can be envisaged: *holodirected*, where the ligand bonded atoms are directed throughout the surface of an encompassing globe, and *hemidirected*, where the ligand bonded atoms are directed throughout a limited part of the globe, so that there is an identifiable void (or gap) in the distribution of bonds to the ligands, see Scheme 1. We hereafter classify the investigated structures in terms of the overall

coordination number, number of iodide ligands, and coordination type. On overall, we investigated eight initial coordination geometries for the $[PbX_n]^{2+}$ complexes, specifically hemidirected structures **3,0-a**; **4,0-a**; **5,0-a**; **6,0-a** in Scheme S1 and holodirected structures **3,0-b**; **4,0-b**; **5,0-b**; **6,0-b** in Scheme S2. Among these, we report in Figure 2a the energetically favored structures (see also Scheme 1). In agreement with the results from crystallographic data and *ab initio* calculations,[59] we found that Pb^{2+} complexes prefer a hemidirected configuration for low cn, up to 3-5. For the cn=6 case, *i.e.* for the $[PbX_6]^{2+}$ complex, both the hemidirected and holodirected coordination gave rise to stable structures, the former being favored by 0.17 eV.
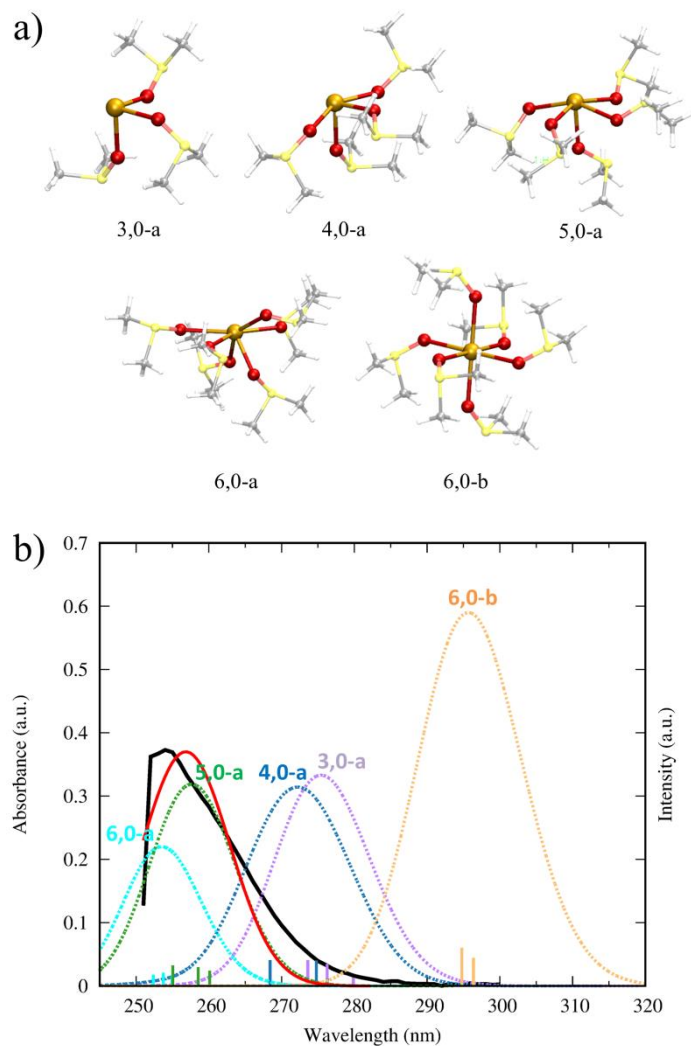
Figure 2. a) Optimized geometrical structures for the $[PbX_n]^{2+}$ (n=3-6, X=DMSO) complexes; b) their TD-DFT computed spectra (6 lowest in energy excited states) (colored dashed lines, intensity vs wavelength) compared to experimental spectrum of $Pb(NO_3)_2$ 0.1 mM in DMSO (solid black line, absorbance vs wavelength). The solid red line refers to a fit of **5,0-a** and **6,0-a** spectra to the experimental one.

For the more stable $[PbX_n]^{2+}$ (X=DMSO) complexes of Figure 2a, we simulated the UV-Vis absorption spectra by TD-DFT employing SOC, by computing several excitation energies and oscillator strengths. The results are reported in Figure 2b, together with the experimental $Pb(NO_3)_2$ spectrum in DMSO for a direct comparison. Remarkably, the number of coordinated DMSO molecules strongly affects the absorption maxima energy. In particular, **3,0-a** shows an absorption

maximum at 275 nm, that slightly shifts to 272 nm for **4,0-a** and shifts further to 254 for **5,0-a**. For a coordination number equal to 6 a strong difference is found for hemidirected and holodirected $[PbX_6]^{2+}$ complexes **6,0-a** and **6,0-b**, characterized respectively by calculated absorption maxima at 258 and 296 nm. Comparing the calculated spectra to the experimental data showing an absorption maximum at 257 nm, we conclude that the solution composition is dominated by **6,0-a,** with a possible contribution from **5,0-a,** thus suggesting that the Pb^{2+} ion preferentially coordinates 5-6 DMSO solvent molecules, with coordination number equal to 6 dominated by the hemidirected coordination. A fit of the experimental spectrum with the computed **6,0-a** and **5-0-a** [see Figure 2 b)] was carried out considering a linear combination of the two gaussian functions that describe our theoretical spectra, as reported here:

$$c_1 * (y_{0,1} + A_1 * \frac{\sqrt{2/\pi}}{w_1} * e^{\left(\frac{-2*(x - x_{c,1})}{w_1}\right)^2}) + c_2 * (y_{0,2} + A_2 * \frac{\sqrt{2/\pi}}{w_2} * e^{\left(\frac{-2*(x - x_{c,2})}{w_2}\right)^2}) \qquad (3)$$

where the parameters with the subscript 1 refer to the **5,0-a** spectrum while those with the subscript 2 are for the **6,0-a**. The optimization was performed only on the linear combination coefficients c_1 and c_2 through an iterative algorithm (scaled Levenberg-Marquardt), that resulted in absolute values of 0.4054 and 0.9382 respectively for c_1 and c_2, thus suggesting the higher contribution of the **6,0-a** spectrum to the experimental one.

Our finding is in agreement with the work of Persson *et al.,*[60] showing the hemidirected $[PbX_6]^{2+}$ complex to be the main species found in a DMSO solution of $Pb(NO_3)_2$, thus confirming the quality of the employed theoretical setup and making us confident on the subsequent assignments.

As outlined above, by adding increasing amounts of MAI to the Pb^{2+} salt solution, the formation of various iodoplumbate complexes, $[PbI_mX_n]^{2-m}$ with m=1-4 is surmised. Our results on the $[PbX_n]^{2+}$ (X=DMSO) complexes highlight the key role of the coordinating solvent molecules on the optical properties of the ensuing complexes. Accordingly, we carried out geometry optimizations of the hypothesized iodoplumbate complexes including in the coordination sphere an

increasing number of solvent molecules. It is worth noting that the presence of two different ligands in the Pb^{2+} coordination sphere, namely the halogen I and the solvent X, increases the possible coordination geometries of the solvated iodoplumbate complexes. On overall, we attempted 29 and 24 distinct hemidirected and holodirected configurations, respectively (see Schemes S1 and S2 in the SI); in Scheme 1 the most energetically stable structures are drawn. Notably, the stability of the various complexes depends on the nature of the solvent, see Scheme 1. Shimoni-Livny *et al*.[59] carried out an extended analysis on the coordination geometry of divalent lead compounds by crystallographic data and *ab initio* calculations, concluding that Pb^{2+} complexes prefer hemidirected and holodirected configuration for low and high coordination number, respectively. For intermediate coordination number values, both holodirected and hemidirected coordinations are found, but the holodirected geometry tends to prevail for iodide ligands. Our results are substantially in agreement with these findings, even if some differences are found, in dependence of the solvent employed in the coordination sphere. The relative formation energies for different complexes are reported against the number of solvent molecules in Figure 3.
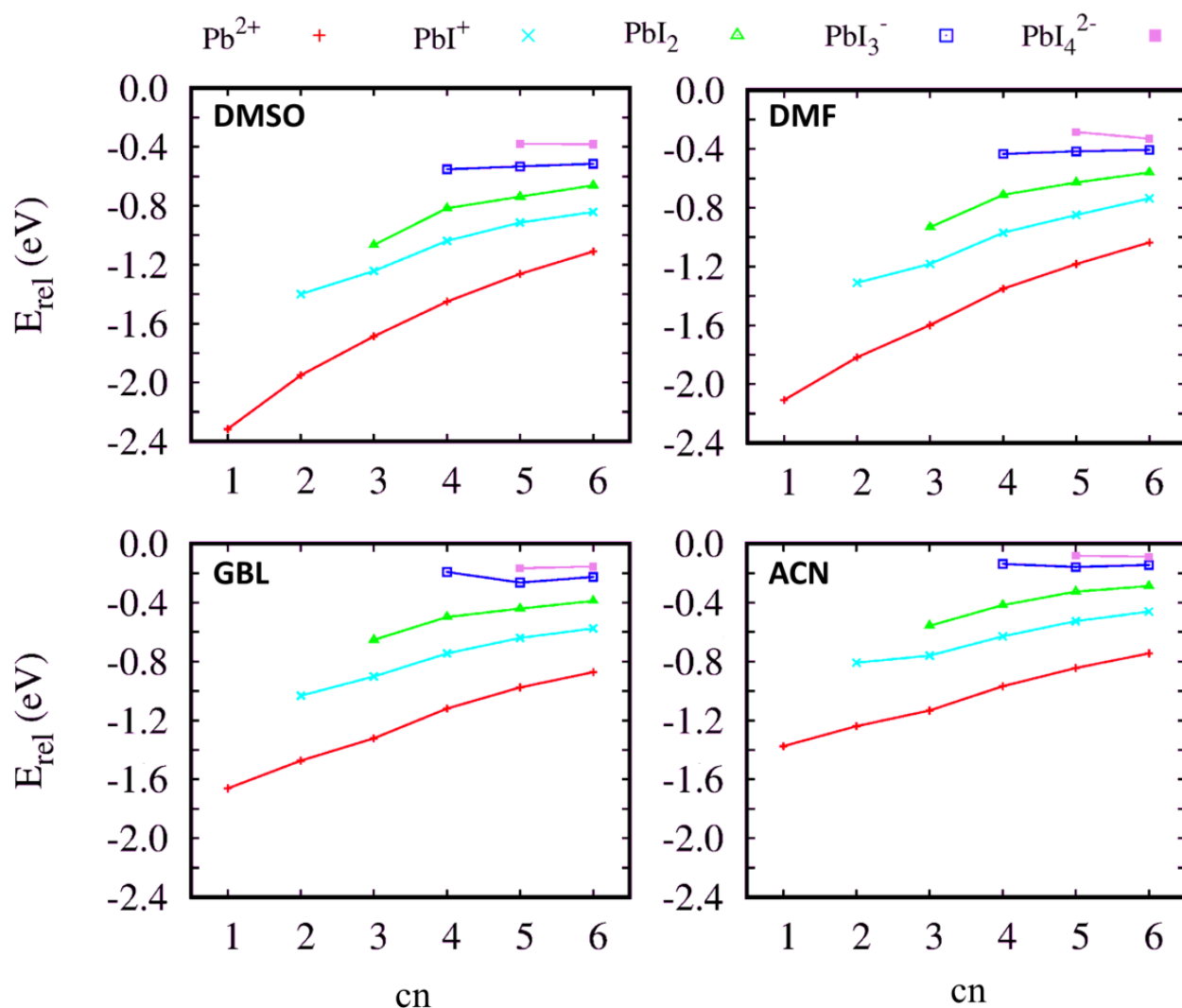
Figure 3. Relative formation energies (E_{rel}, in eV) of solvated iodoplumbates $[PbI_mX_n]^{2-m}$ vs the total coordination number (cn), for various employed solvents.

As it can be noticed, DMSO shows the highest stabilization energy upon coordination for each iodoplumbate complex, followed by DMF, GBL and ACN. The computed values for the iodoplumbate energy solvation can be related to the solvent coordinative power, since higher energy stabilization values correspond to higher coordinative powers. On the basis of the energy values in Figure 3, the following trend for the energy solvation can be envisaged: DMSO > DMF > GBL > ACN, that is in fairly good agreement with the well-known coordinative solvent power.[58,61–64] Interestingly, the experimental solubility of PbI_2 in the various solvents (see Table S4) follows the

same trend, as also reported by Stevenson *et al.*,[65] in line with the expected relation between solvent coordination ability and Pb^{2+} solubility and with the donor number of the solvents.[57,66]

To correlate the obtained theoretical and experimental findings, we carried out the simulation of the absorption spectra for the $[PbI_mX_n]^{2-m}$ iodoplumbate complexes (X= DMSO and DMF) that were computed to be more stable in energy, as per Scheme 1. In particular, in Figures 4 and 5 we report the absorption spectra of selected $[PbI_mX_n]^{2-m}$ iodoplumbate complexes, that most resemble the experimental spectra of lead salt solutions with the addition of MAI, respectively for DMSO and DMF. Other simulated absorption spectra are shown in the SI.
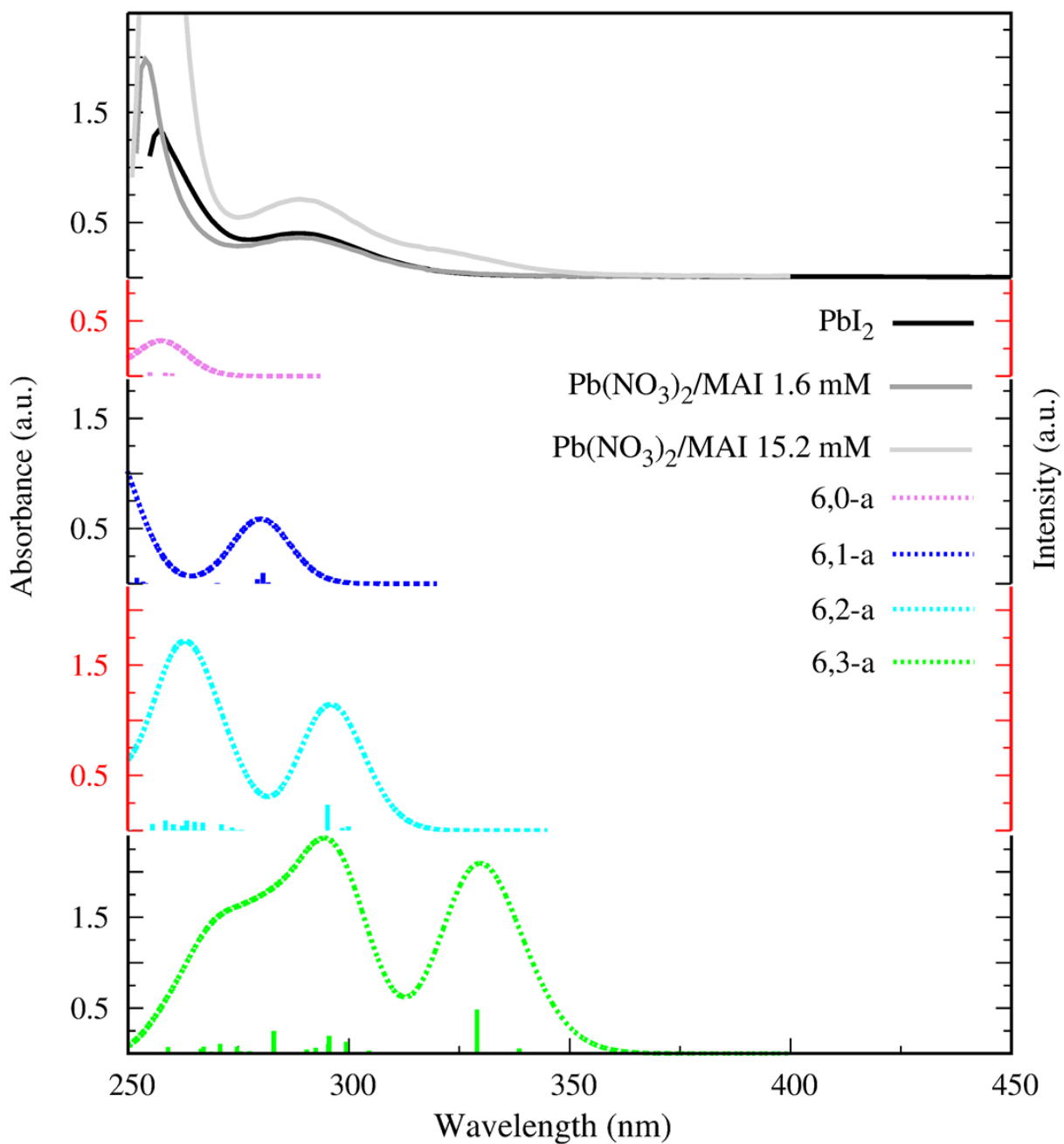
Figure 4. Comparison between computed (dotted lines) absorption spectra for selected $[PbI_mX_n]^{2-m}$ iodoplumbate complexes and experimental UV-Vis (solid lines) absorption spectra of PbI_2 solution without addition of MAI and $Pb(NO_3)_2$ solution with the addition of MAI 1.6 / 15.2 mM in DMSO.
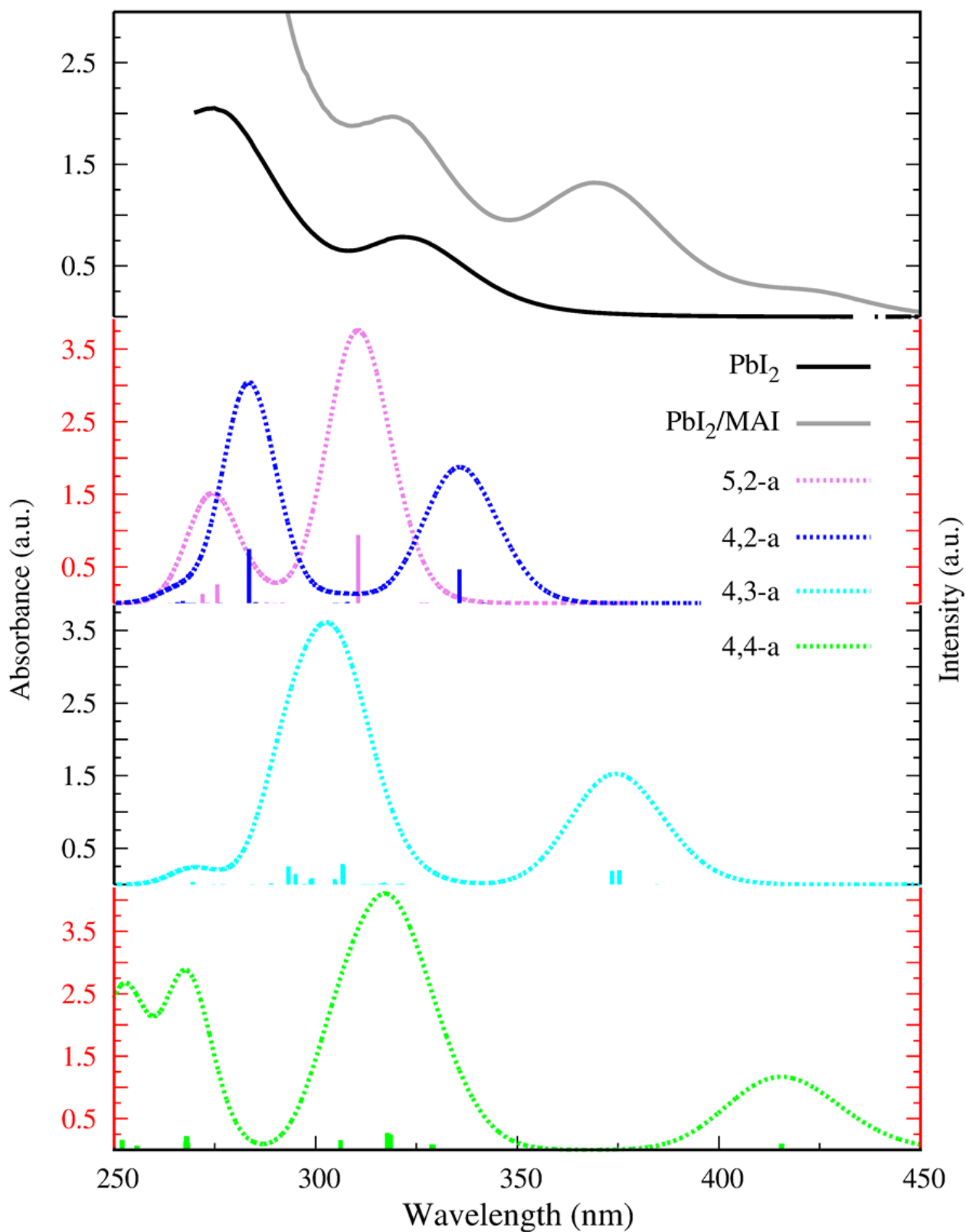
Figure 5. Comparison between computed (dotted lines) absorption spectra for selected $[PbI_mX_n]^{2-m}$ iodoplumbate complexes and experimental UV-Vis (solid lines) absorption spectra of PbI_2 solution without and with the addition of MAI 24.0 mM in DMF.

As already discussed, we can see that the experimental spectra of lead solutions show two absorption features, at 257/290 nm in DMSO (Figure 4) and 275/323 nm in DMF (Figure 5). Interestingly, the PbI_2X_4 **6,2-a** spectrum, see structure in Figure 6, well describes the experimental spectrum of lead solutions in DMSO, with calculated absorption maxima at 264/295 nm against experimental values of 257/290 nm (see Figure 4). In DMF the spectrum that more closely matches the experimental one is that of PbI_2X_3 **5,2-a**, see structure in Figure 6, with absorption maxima of 275/311 nm against 275/323 nm experimental values, though the spectrum of PbI_2X_2 **4,2-a** is also quite close to the experimental one (see Figure 5). Remarkably, a coordination number equal to 6 was found for other Pb salts in DMF, [60] thus suggesting that the total coordination number could be could be significantly dependent on the ligand coordination sphere.

A comparison of pseudo-octahedral structures with increasing number of iodide ligands in DMSO, namely $[PbX_6]^{2+}$ **6,0-a**, $[PbIX_5]^+$ **6,1-a**, PbI_2X_4 **6,2-a** and $[PbI_3X_3]^-$ **6,3-a**, is reported in Figure 6. As discussed above and reported in Figure 4, the $[PbX_6]^{2+}$ **6,0-a** complex shows a peak centered at 257 nm. As expected, when considering the excitations for the other iodoplumbate complexes, several absorption bands appear at shorter wavelengths. In particular, for the $[PbIX_5]^+$ **6,1-a** complex, we computed a strong absorption band centered at 240 nm, together with a peak at 280 nm. As reported before, also for the PbI_2X_4 **6,2-a** complex we computed two peaks, at 264 and 295 nm. Remarkably, the absorption spectrum of the $[PbI_3X_3]^-$ **6,3-a** complex strongly differs from that of the other species, since it shows a peak at 295 nm, with a shoulder at 270 nm, and another at 329 nm, with very high intensity. This last feature cannot be seen from the experimental spectrum of a 0.24 mM PbI_2 solution, but appears when a relatively high quantity of MAI is added to $Pb(NO_3)_2$ 0.1mM (see Figure 1). According to the present results, we can surmise that the experimental peak centered at 290 nm (see Figure 1) can be related to the $[PbI_3X_3]^-$, PbI_2X_4 and $[PbIX_5]^+$ complexes, while the experimental peak centered at 320 nm can be related exclusively to the $[PbI_3X_3]^-$ complex.
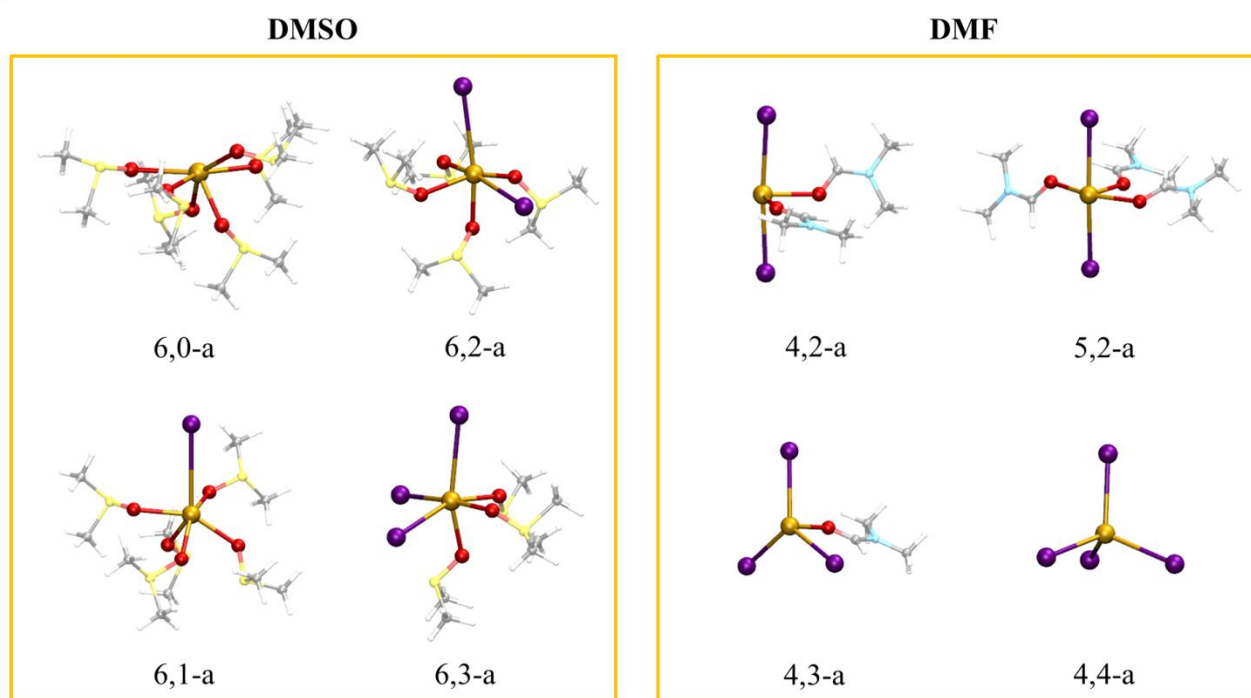
For the iodoplumbate complexes in DMF solvent with the addition of MAI, we selected three structures, one with coordination number equal to 5, PbI_2X_3 **5,2-a**, that we already presented earlier for the excellent agreement with the experimental bands, and two with coordination number equal to 4, $[PbI_3X]^-$ **4,3-a** and $[PbI_4]^{2-}$ **4,4-a** without coordinating DMF molecules, see Figure 6. For the $[PbI_3X]^-$ **4,3-a** complex, we computed a band with low intensity at 270 nm and two other bands centered at 302 and 375 nm. Finally, the $[PbI_4]^{2-}$ **4,4-a** shows two outdistanced peaks at 317 and 416 nm. On the basis of the experimental results reported in Figure 1, we unambiguously assign the peak at 423 nm to the PbI_4^{2-} species, while the peak at 370 nm could result from the absorption of various species, such as $[PbI_4]^{2-}$, $[PbI_3X]^-$ and PbI_2X_3.

A complete overview of the presented experimental and theoretical data is reported in Table 3.

Table 3. Comparison of experimental (Exp) and computed (Th) absorption maxima (nm) of the investigated $[PbI_mX_n]^{2-m}$ structures in DMSO and DMF solvents.

PbI_m^{2-m}	DMSO			DMF		
	Exp	Th		Exp	Th	
Pb^{2+}	257	275 272 254 258 296	(3,0-a) (4,0-a) (5,0-a) (6,0-a) (6,0-b)	/	/	/
PbI^+	257/287	240/280	(6,1-a)	/	/	/
PbI_2	290	254/267/294/317/347 274/340 311 264/295	(3,2-a) (4,2-a) (5,2-a) (6,2-a)	275/323	292/316/345 284/336 275/311 267/292	(3,2-a) (4,2-a) (5,2-a) (6,2-a)
PbI_3^-	320	270/295/329	(6,3-a)	370	270/302/375	(4,3-a)

| PbI$_4{}^{2-}$ | / | / | 423 | 317/416 | (**4,4-a**) |

Figure 6. Optimized geometries for selected [PbI$_m$X$_n$]$^{2-m}$ iodoplumbate complexes in DMSO (left) and DMF (right) solvents.

Our results show that the iodoplumbate species that are most likely to be present in the DMSO solution environment have a higher coordination number than those in DMF, with the consequence that in DMSO iodoplumbates with a lower number of iodide ligands are preferred. In other words, the stronger solvent coordination partially displaces the fairly weak iodide ligands, so that lower iodide complexes are favored in DMSO against DMF. This could be addressed to the higher coordinating ability of DMSO with respect to DMF,[54] and it likely can be extrapolated to other solvents.

The different coordination number and composition of solvated iodoplumbates obtained in different solvents may have important consequences for the kinetics of perovskite formation. As a matter of fact, the stronger Pb-solvent interaction in DMSO will likely slow down the

crystallization process upon evaporating the solvent, since it will be more difficult to abstract solvent molecules from the precursors. In this case, the lower tendency to form species with higher number of iodide ligands may at the same time give rise to a less defective structure, which may minimize the incorporation of extra iodine in the lattice in the form of *e.g.* interstitial iodine. In DMF the preferred species have low coordination number and a comparatively higher iodide content, thus upon the fast solvent evaporation, some of the extra iodide originated by *e.g.* PbI_4^{2-} species, may be transferred to the perovskite lattice with possible detrimental consequences on the material optoelectronic quality. At the same time, the weaker Pb-solvent interaction will likely speed up the formation of crystal grains grown under non-equilibrium conditions, possibly leading to a more disordered material.

4. Conclusions

Uncovering the mechanisms that lead to the formation of the perovskite polycrystalline thin films is crucial in order to understand how these changes reflect in the final perovskite properties and so to be able to improve these properties tuning the solution chemistry. In the present work we have identified the composition of the solvated iodoplumbate complexes involved in a common perovskite precursors DMSO/DMF solution by means of a combined experimental and theoretical strategy. Experimental spectra gave us a view of the species in solution, that were analyzed by fitting software for the evaluation of the spectral shapes and equilibrium constants of the different species. Upon addition of MAI to the lead solution, several absorption bands appear at lower wavelength. The specific molecular interactions between the iodoplumbate complexes, $[PbI_m]^{2-m}$, and the solvent molecules, X, upon addition of MAI were analyzed by identifying the most thermodynamically stable structures in various solvent solutions and characterizing their optical properties trough DFT and TD-DFT calculations. The theoretical strategy was first benchmarked comparing simulated spectra of selected optimized complexes with the experimental UV-Vis spectrum of a $Pb(NO_3)_2$ in DMSO solution. Then, the formation energies of the simulated

complexes and the comparison between experimental and theoretical absorption spectra were used to shed light on the coordinative power of various solvents to the iodoplumbates species and their specific interactions, giving us the possibility to predict the number of iodide ions and of solvent molecules coordinated to the Pb^{2+} center. In this way, we have found that iodoplumbate-DMSO complexes have, on average, a higher coordination number and a lower iodide ligand number with respect to the iodoplumbate-DMF ones. Specifically, the experimental spectra of lead solutions in DMSO are adequately describe by the spectra computed for the PbI_2X_4 **6,2-a**, $[PbI_3X_3]^-$ **6,3-a** and $[PbIX_5]^+$ **6,1-a** structures, while in DMF solvent the spectra that more closely match with the experimental ones are those related to PbI_2X_3 **5,2-a**, PbI_2X_2 **4,2-a**, $[PbI_3X]^-$ **4,3-a** and $[PbI_4]^{2-}$ **4,4-a** structures. Our combined computational and experimental analysis points out the critical role of the nature of the solvent in affecting the perovskite precursor solution, with possible important consequences on the ensuing material optoelectronic quality. As a general conclusion, we illustrate how weaker coordinating solvents give preferentially rise to iodoplumbates with higher iodide content and lower solvent coordinated molecules, with a likely impact on the kinetics of perovskite formation.

Supporting Information Optimized structures and experimental and simulated absorption spectra for the investigated iodoplumbate complexes.

Acknowledgements

References

(1)   Snaith, H. J. Perovskites: The Emergence of a New Era for Low-Cost, High-Efficiency Solar Cells. *J. Phys. Chem. Lett.* **2013**, *4* (21), 3623–3630. https://doi.org/10.1021/jz4020162.

(2)   Green, M. A.; Ho-Baillie, A.; Snaith, H. J. The Emergence of Perovskite Solar Cells. *Nat. Photonics* **2014**, *8* (7), 506–514. https://doi.org/10.1038/nphoton.2014.134.

(3)   Photovoltaic Research | NREL https://www.nrel.gov/pv/.

(4)   Lin, Q.; Armin, A.; Burn, P. L.; Meredith, P. Organohalide Perovskites for Solar Energy Conversion. *Acc. Chem. Res.* **2016**, *49* (3), 545–553. https://doi.org/10.1021/acs.accounts.5b00483.

(5)   Zhao, Y.; Zhu, K. Solution Chemistry Engineering toward High-Efficiency Perovskite Solar Cells. *J. Phys. Chem. Lett.* **2014**, *5* (23), 4175–4186. https://doi.org/10.1021/jz501983v.

(6)   Yang, M.; Zhang, T.; Schulz, P.; Li, Z.; Li, G.; Kim, D. H.; Guo, N.; Berry, J. J.; Zhu, K.; Zhao, Y. Facile Fabrication of Large-Grain $CH_3NH_3PbI_{3-x}Br_x$ Films for High-Efficiency Solar Cells via CH_3NH_3Br-Selective Ostwald Ripening. *Nat. Commun.* **2016**, *7*, 12305. https://doi.org/10.1038/ncomms12305.

(7)   Etgar, L.; Gao, P.; Xue, Z.; Peng, Q.; Chandiran, A. K.; Liu, B.; Nazeeruddin, Md. K.; Grätzel, M. Mesoscopic $CH_3NH_3PbI_3$/TiO_2 Heterojunction Solar Cells. *J. Am. Chem. Soc.* **2012**, *134* (42), 17396–17399. https://doi.org/10.1021/ja307789s.

(8)   Seo, J.; Park, S.; Kim, Y. C.; Jeon, N. J.; Noh, J. H.; Yoon, S. C.; Seok, S. I. Benefits of Very Thin PCBM and LiF Layers for Solution-Processed p–i–n Perovskite Solar Cells. *Energy Environ. Sci.* **2014**, *7* (8), 2642–2646. https://doi.org/10.1039/C4EE01216J.

(9)   Manser, J. S.; Reid, B.; Kamat, P. V. Evolution of Organic–Inorganic Lead Halide Perovskite from Solid-State Iodoplumbate Complexes. *J. Phys. Chem. C* **2015**, *119* (30), 17065–17073. https://doi.org/10.1021/acs.jpcc.5b05898.

(10)   Moore, D. T.; Sai, H.; Tan, K. W.; Smilgies, D.-M.; Zhang, W.; Snaith, H. J.; Wiesner, U.; Estroff, L. A. Crystallization Kinetics of Organic–Inorganic Trihalide Perovskites and the Role of the Lead Anion in Crystal Growth. *J. Am. Chem. Soc.* **2015**, *137* (6), 2350–2358. https://doi.org/10.1021/ja512117e.

(11)   Williams, S. T.; Zuo, F.; Chueh, C.-C.; Liao, C.-Y.; Liang, P.-W.; Jen, A. K.-Y. Role of Chloride in the Morphological Evolution of Organo-Lead Halide Perovskite Thin Films. *ACS Nano* **2014**, *8* (10), 10640–10654. https://doi.org/10.1021/nn5041922.

(12)   Colella, S.; Mosconi, E.; Fedeli, P.; Listorti, A.; Gazza, F.; Orlandi, F.; Ferro, P.; Besagni, T.; Rizzo, A.; Calestani, G.; et al. $MAPbI_{3-x}Cl_x$ Mixed Halide Perovskite for Hybrid Solar Cells: The Role of Chloride as Dopant on the Transport and Structural Properties. *Chem. Mater.* **2013**, *25* (22), 4613–4618. https://doi.org/10.1021/cm402919x.

(13)   Ahn, N.; Son, D.-Y.; Jang, I.-H.; Kang, S. M.; Choi, M.; Park, N.-G. Highly Reproducible Perovskite Solar Cells with Average Efficiency of 18.3% and Best Efficiency of 19.7% Fabricated via Lewis Base Adduct of Lead(II) Iodide. *J. Am. Chem. Soc.* **2015**, *137* (27), 8696–8699. https://doi.org/10.1021/jacs.5b04930.

(14)   Yang, W. S.; Noh, J. H.; Jeon, N. J.; Kim, Y. C.; Ryu, S.; Seo, J.; Seok, S. I. High-Performance Photovoltaic Perovskite Layers Fabricated Through Intramolecular Exchange. *Science* **2015**, *348* (6240), 1234–1237. https://doi.org/10.1126/science.aaa9272.

(15)   Guo, Y.; Shoyama, K.; Sato, W.; Matsuo, Y.; Inoue, K.; Harano, K.; Liu, C.; Tanaka, H.; Nakamura, E. Chemical Pathways Connecting Lead(II) Iodide and Perovskite via Polymeric Plumbate(II) Fiber. *J. Am. Chem. Soc.* **2015**, *137* (50), 15907–15914. https://doi.org/10.1021/jacs.5b10599.

(16)   Yan, K.; Long, M.; Zhang, T.; Wei, Z.; Chen, H.; Yang, S.; Xu, J. Hybrid Halide Perovskite Solar Cell Precursors: Colloidal Chemistry and Coordination Engineering behind Device Processing for High Efficiency. *J. Am. Chem. Soc.* **2015**, *137* (13), 4460–4468. https://doi.org/10.1021/jacs.5b00321.

(17)   Zhao, Y.; Zhu, K. CH_3NH_3Cl-Assisted One-Step Solution Growth of $CH_3NH_3PbI_3$: Structure, Charge-Carrier Dynamics, and Photovoltaic Properties of Perovskite Solar Cells. *J. Phys. Chem. C* **2014**, *118* (18), 9412–9418. https://doi.org/10.1021/jp502696w.

(18)   McMeekin, D. P.; Wang, Z.; Rehman, W.; Pulvirenti, F.; Patel, J. B.; Noel, N. K.; Johnston, M. B.; Marder, S. R.; Herz, L. M.; Snaith, H. J. Crystallization Kinetics and Morphology Control of

Formamidinium–Cesium Mixed-Cation Lead Mixed-Halide Perovskite via Tunability of the Colloidal Precursor Solution. *Adv. Mater.* **2017**, *29* (29), 1607039. https://doi.org/10.1002/adma.201607039.

(19) Noel, N. K.; Congiu, M.; Ramadan, A. J.; Fearn, S.; McMeekin, D. P.; Patel, J. B.; Johnston, M. B.; Wenger, B.; Snaith, H. J. Unveiling the Influence of PH on the Crystallization of Hybrid Perovskites, Delivering Low Voltage Loss Photovoltaics. *Joule* **2017**, *1* (2), 328–343. https://doi.org/10.1016/j.joule.2017.09.009.

(20) Ramadan, A. J.; Noel, N. K.; Fearn, S.; Young, N.; Walker, M.; Rochford, L. A.; Snaith, H. J. Unravelling the Improved Electronic and Structural Properties of Methylammonium Lead Iodide Deposited from Acetonitrile. *Chem. Mater.* **2018**, *30* (21), 7737–7743. https://doi.org/10.1021/acs.chemmater.8b03084.

(21) Tidhar, Y.; Edri, E.; Weissman, H.; Zohar, D.; Hodes, G.; Cahen, D.; Rybtchinski, B.; Kirmayer, S. Crystallization of Methyl Ammonium Lead Halide Perovskites: Implications for Photovoltaic Applications. *J. Am. Chem. Soc.* **2014**, *136* (38), 13249–13256. https://doi.org/10.1021/ja505556s.

(22) Mosconi, E.; Ronca, E.; De Angelis, F. First-Principles Investigation of the TiO_2/Organohalide Perovskites Interface: The Role of Interfacial Chlorine. *J. Phys. Chem. Lett.* **2014**, *5* (15), 2619–2625. https://doi.org/10.1021/jz501127k.

(23) Grancini, G.; Marras, S.; Prato, M.; Giannini, C.; Quarti, C.; De Angelis, F.; De Bastiani, M.; Eperon, G. E.; Snaith, H. J.; Manna, L.; et al. The Impact of the Crystallization Processes on the Structural and Optical Properties of Hybrid Perovskite Films for Photovoltaics. *J. Phys. Chem. Lett.* **2014**, *5* (21), 3836–3842. https://doi.org/10.1021/jz501877h.

(24) Jeon, N. J.; Noh, J. H.; Kim, Y. C.; Yang, W. S.; Ryu, S.; Seok, S. I. Solvent Engineering for High-Performance Inorganic–Organic Hybrid Perovskite Solar Cells. *Nat. Mater.* **2014**, *13* (9), 897–903. https://doi.org/10.1038/nmat4014.

(25) Cao, J.; Jing, X.; Yan, J.; Hu, C.; Chen, R.; Yin, J.; Li, J.; Zheng, N. Identifying the Molecular Structures of Intermediates for Optimizing the Fabrication of High-Quality Perovskite Films. *J. Am. Chem. Soc.* **2016**, *138* (31), 9919–9926. https://doi.org/10.1021/jacs.6b04924.

(26) Wu, Y.; Islam, A.; Yang, X.; Qin, C.; Liu, J.; Zhang, K.; Peng, W.; Han, L. Retarding the Crystallization of PbI_2 for Highly Reproducible Planar-Structured Perovskite Solar Cells via Sequential Deposition. *Energy Environ. Sci.* **2014**, *7* (9), 2934–2938. https://doi.org/10.1039/C4EE01624F.

(27) Miyamae, H.; Numahata, Y.; Nagata, M. The Crystal Structure of Lead(II) Iodide-Dimethylsulphoxide(1/2), $PbI_2(DMSO)_2$. *Chem. Lett.* **1980**, *9* (6), 663–664. https://doi.org/10.1246/cl.1980.663.

(28) Wakamiya, A.; Endo, M.; Sasamori, T.; Tokitoh, N.; Ogomi, Y.; Hayase, S.; Murata, Y. Reproducible Fabrication of Efficient Perovskite-Based Solar Cells: X-Ray Crystallographic Studies on the Formation of $CH_3NH_3PbI_3$ Layers. *Chem. Lett.* **2014**, *43* (5), 711–713. https://doi.org/10.1246/cl.140074.

(29) Petrov, A. A.; Sokolova, I. P.; Belich, N. A.; Peters, G. S.; Dorovatovskii, P. V.; Zubavichus, Y. V.; Khrustalev, V. N.; Petrov, A. V.; Grätzel, M.; Goodilin, E. A.; et al. Crystal Structure of DMF-Intermediate Phases Uncovers the Link Between $CH_3NH_3PbI_3$ Morphology and Precursor's Stoichiometry. *J. Phys. Chem. C* **2017**, *121* (38), 20739–20743. https://doi.org/10.1021/acs.jpcc.7b08468.

(30) Fateev, S. A.; Petrov, A. A.; Khrustalev, V. N.; Dorovatovskii, P. V.; Zubavichus, Y. V.; Goodilin, E. A.; Tarasov, A. B. Solution Processing of Methylammonium Lead Iodide Perovskite from γ-Butyrolactone: Crystallization Mediated by Solvation Equilibrium. *Chem. Mater.* **2018**, *30* (15), 5237–5244. https://doi.org/10.1021/acs.chemmater.8b01906.

(31) Paek, S.; Schouwink, P.; Athanasopoulou, E. N.; Cho, K. T.; Grancini, G.; Lee, Y.; Zhang, Y.; Stellacci, F.; Nazeeruddin, M. K.; Gao, P. From Nano- to Micrometer Scale: The Role of Antisolvent Treatment on High Performance Perovskite Solar Cells. *Chem. Mater.* **2017**, *29* (8), 3490–3498. https://doi.org/10.1021/acs.chemmater.6b05353.

(32) Shi, D.; Adinolfi, V.; Comin, R.; Yuan, M.; Alarousu, E.; Buin, A.; Chen, Y.; Hoogland, S.; Rothenberger, A.; Katsiev, K.; et al. Low Trap-State Density and Long Carrier Diffusion in Organolead Trihalide Perovskite Single Crystals. *Science* **2015**, *347* (6221), 519–522. https://doi.org/10.1126/science.aaa2725.

(33)   Zhang, Y.; Gao, P.; Oveisi, E.; Lee, Y.; Jeangros, Q.; Grancini, G.; Paek, S.; Feng, Y.; Nazeeruddin, M. K. PbI$_2$–HMPA Complex Pretreatment for Highly Reproducible and Efficient CH$_3$NH$_3$PbI$_3$ Perovskite Solar Cells. *J. Am. Chem. Soc.* **2016**, *138* (43), 14380–14387. https://doi.org/10.1021/jacs.6b08347.

(34)   Zhi, L.; Li, Y.; Cao, X.; Li, Y.; Cui, X.; Ci, L.; Wei, J. Perovskite Solar Cells Fabricated by Using an Environmental Friendly Aprotic Polar Additive of 1,3-Dimethyl-2-Imidazolidinone. *Nanoscale Res. Lett.* **2017**, *12* (1), 632. https://doi.org/10.1186/s11671-017-2391-3.

(35)   Li, W.; Fan, J.; Li, J.; Mai, Y.; Wang, L. Controllable Grain Morphology of Perovskite Absorber Film by Molecular Self-Assembly toward Efficient Solar Cell Exceeding 17%. *J. Am. Chem. Soc.* **2015**, *137* (32), 10399–10405. https://doi.org/10.1021/jacs.5b06444.

(36)   Manser, J. S.; Saidaminov, M. I.; Christians, J. A.; Bakr, O. M.; Kamat, P. V. Making and Breaking of Lead Halide Perovskites. *Acc. Chem. Res.* **2016**, *49* (2), 330–338. https://doi.org/10.1021/acs.accounts.5b00455.

(37)   Stewart, R. J.; Grieco, C.; Larsen, A. V.; Doucette, G. S.; Asbury, J. B. Molecular Origins of Defects in Organohalide Perovskites and Their Influence on Charge Carrier Dynamics. *J. Phys. Chem. C* **2016**, *120* (23), 12392–12402. https://doi.org/10.1021/acs.jpcc.6b03472.

(38)   Stamplecoskie, K. G.; Manser, J. S.; Kamat, P. V. Dual Nature of the Excited State in Organic–Inorganic Lead Halide Perovskites. *Energy Environ. Sci.* **2015**, *8* (1), 208–215. https://doi.org/10.1039/C4EE02988G.

(39)   Seok, S. I.; Grätzel, M.; Park, N.-G. Methodologies toward Highly Efficient Perovskite Solar Cells. *Small* **2018**, *14* (20), 1704177. https://doi.org/10.1002/smll.201704177.

(40)   Rahimnejad, S.; Kovalenko, A.; Forés, S. M.; Aranda, C.; Guerrero, A. Coordination Chemistry Dictates the Structural Defects in Lead Halide Perovskites. *ChemPhysChem* **2016**, *17* (18), 2795–2798. https://doi.org/10.1002/cphc.201600575.

(41)   Cao, X. B.; Li, C. L.; Zhi, L. L.; Li, Y. H.; Cui, X.; Yao, Y. W.; Ci, L. J.; Wei, J. Q. Fabrication of High Quality Perovskite Films by Modulating the Pb–O Bonds in Lewis Acid–Base Adducts. *J. Mater. Chem. A* **2017**, *5* (18), 8416–8422. https://doi.org/10.1039/C7TA00539C.

(42)   Yoon, S. J.; Stamplecoskie, K. G.; Kamat, P. V. How Lead Halide Complex Chemistry Dictates the Composition of Mixed Halide Perovskites. *J. Phys. Chem. Lett.* **2016**, *7* (7), 1368–1373. https://doi.org/10.1021/acs.jpclett.6b00433.

(43)   Mastria, R.; Colella, S.; Qualtieri, A.; Listorti, A.; Gigli, G.; Rizzo, A. Elucidating the Effect of the Lead Iodide Complexation Degree Behind the Morphology and Performance of Perovskite Solar Cells. *Nanoscale* **2017**, *9* (11), 3889–3897. https://doi.org/10.1039/C6NR09819C.

(44)   Masi, S.; Aiello, F.; Listorti, A.; Balzano, F.; Altamura, D.; Giannini, C.; Caliandro, R.; Uccello-Barretta, G.; Rizzo, A.; Colella, S. Connecting the Solution Chemistry of PbI$_2$ and MAI: A Cyclodextrin-Based Supramolecular Approach to the Formation of Hybrid Halide Perovskites. *Chem. Sci.* **2018**, *9* (12), 3200–3208. https://doi.org/10.1039/C7SC05095J.

(45)   Sharenko, A.; Mackeen, C.; Jewell, L.; Bridges, F.; Toney, M. F. Evolution of Iodoplumbate Complexes in Methylammonium Lead Iodide Perovskite Precursor Solutions. *Chem. Mater.* **2017**, *29* (3), 1315–1320. https://doi.org/10.1021/acs.chemmater.6b04917.

(46)   Frisch, M. J.; Trucks, G. W.; Schlegel, H. B.; Scuseria, G. E.; Robb, M. A.; Cheeseman, J. R.; Scalmani, G.; Barone, V.; Petersson, G. A.; Nakatsuji, H.; et al. *Gaussian 09, Revision D. 01*; Gaussian, Inc., Wallingford CT, 2016.

(47)   te Velde, G.; Bickelhaupt, F. M.; Baerends, E. J.; Fonseca Guerra, C.; van Gisbergen, S. J. A.; Snijders, J. G.; Ziegler, T. Chemistry with ADF. *J. Comput. Chem.* **2001**, *22* (9), 931–967. https://doi.org/10.1002/jcc.1056.

(48)   Fonseca Guerra, C.; Snijders, J. G.; te Velde, G.; Baerends, E. J. Towards An Order-N DFT Method. *Theor. Chem. Acc.* **1998**, *99* (6), 391–403. https://doi.org/10.1007/s002140050353.

(49)   ADF 2014, SCM, Theoretical Chemistry, Vrije Universiteit, Amsterdam, The Netherlands, http://www.scm.com.

(50)   van Lenthe, E.; Baerends, E. J.; Snijders, J. G. Relativistic Regular Two-Component Hamiltonians. *J. Chem. Phys.* **1993**, *99* (6), 4597–4610. https://doi.org/10.1063/1.466059.

(51) Wang, F.; Ziegler, T.; van Lenthe, E.; van Gisbergen, S.; Baerends, E. J. The Calculation of Excitation Energies Based on the Relativistic Two-Component Zeroth-Order Regular Approximation and Time-Dependent Density-Functional with Full Use of Symmetry. *J. Chem. Phys.* **2005**, *122* (20), 204103. https://doi.org/10.1063/1.1899143.

(52) Becke, A. D. Density-Functional Thermochemistry. III. The Role of Exact Exchange. *J. Chem. Phys.* **1993**, *98* (7), 5648–5652. https://doi.org/10.1063/1.464913.

(53) Stephens, P. J.; Devlin, F. J.; Chabalowski, C. F.; Frisch, M. J. Ab Initio Calculation of Vibrational Absorption and Circular Dichroism Spectra Using Density Functional Force Fields. *J. Phys. Chem.* **1994**, *98* (45), 11623–11627. https://doi.org/10.1021/j100096a001.

(54) Nunzi, F.; De Angelis, F.; Selloni, A. Ab Initio Simulation of the Absorption Spectra of Photoexcited Carriers in TiO_2 Nanoparticles. *J. Phys. Chem. Lett.* **2016**, *7* (18), 3597–3602. https://doi.org/10.1021/acs.jpclett.6b01517.

(55) Nunzi, F.; Fantacci, S.; Cariati, E.; Tordin, E.; Casati, N.; Macchi, P. Stabilization Through P-Dimethylaminobenzaldehyde of a New NLO-Active Phase of [E-4-(4-Dimethylaminostyryl)-1-Methylpyridinium] Iodide: Synthesis, Structural Characterization and Theoretical Investigation of Its Electronic Properties. *J. Mater. Chem.* **2010**, *20* (36), 7652–7660. https://doi.org/10.1039/c0jm00466a.

(56) ReactLab Equilibria | Jplus Consulting http://jplusconsulting.com/products/reactlab-equilibria/ (accessed Apr 10, 2017).

(57) Hamill, J. C.; Schwartz, J.; Loo, Y.-L. Influence of Solvent Coordination on Hybrid Organic–Inorganic Perovskite Formation. *ACS Energy Lett.* **2018**, *3* (1), 92–97. https://doi.org/10.1021/acsenergylett.7b01057.

(58) Gutmann, V. Coordination Chemistry of Certain Transition Metal Ions in Donor Solvents. In *Coordination Chemistry in Non-Aqueous Solutions*; Gutmann, V., Ed.; Springer Vienna: Vienna, 1968; pp 161–168.

(59) Shimoni-Livny, L.; Glusker, J. P.; Bock, C. W. Lone Pair Functionality in Divalent Lead Compounds. *Inorg. Chem.* **1998**, *37* (8), 1853–1867. https://doi.org/10.1021/ic970909r.

(60) Persson, I.; Lyczko, K.; Lundberg, D.; Eriksson, L.; Płaczek, A. Coordination Chemistry Study of Hydrated and Solvated Lead(II) Ions in Solution and Solid State. *Inorg. Chem.* **2011**, *50* (3), 1058–1072. https://doi.org/10.1021/ic1017714.

(61) Gritzner, G. A Critical View on the Lewis-Donor (Nucleophilic) Properties of Solvents. *J. Mol. Liq.* **1997**, *73–74*, 487–500. https://doi.org/10.1016/S0167-7322(97)00090-1.

(62) Persson, I.; Sandström, M.; Goggin, P. L. On the Coordinating Properties of Some Solvents. A Vibrational Spectroscopic Study of Mercury(II) Halides and Antimony(V) Chloride in Solution; New Concepts for Lewis Basicity Scales of Solvents. *Inorganica Chim. Acta* **1987**, *129* (2), 183–197. https://doi.org/10.1016/S0020-1693(00)86662-1.

(63) Munakata, M.; Kitagawa, S.; Miyazima, M. Classification of Solvents Based on Their Coordination Power to Nickel(II) Ion. A New Measure for Solvent Donor Ability. *Inorg. Chem.* **1985**, *24* (11), 1638–1643. https://doi.org/10.1021/ic00205a009.

(64) Munakata, M.; Kitagawa, S. Coordination Power Series of Solvents: 2. The Solvent Effects on Complex Formations, Half-Wave Potentials, ^{113}Cd NMR Resonances and Gibbs Free Energy Changes of Transfer. *Inorganica Chim. Acta* **1990**, *169* (2), 225–234. https://doi.org/10.1016/S0020-1693(00)80522-8.

(65) Stevenson, J.; Sorenson, B.; Subramaniam, V. H.; Raiford, J.; Khlyabich, P. P.; Loo, Y.-L.; Clancy, P. Mayer Bond Order as a Metric of Complexation Effectiveness in Lead Halide Perovskite Solutions. *Chem. Mater.* **2017**, *29* (6), 2435–2444. https://doi.org/10.1021/acs.chemmater.6b04327.

(66) Fawcett, W. R. Acidity and Basicity Scales for Polar Solvents. *J. Phys. Chem.* **1993**, *97* (37), 9540–9546. https://doi.org/10.1021/j100139a045.

Table of Contents